Journal of Power Sources 195 (2010) 1516–1521

Contents lists available at ScienceDirect

Journal of Power Sources

journal homepage: www.elsevier.com/locate/jpowsour

Short communication

A doped activated carbon prepared from polyaniline for high performance supercapacitors

Limin Li, Enhui Liu*, Jian Li, Yanjing Yang, Haijie Shen, Zhengzheng Huang, Xiaoxia Xiang, Wen Li

Key Laboratory of Environmentally Friendly Chemistry and Applications of Ministry of Education, College of Chemistry, Xiangtan University, Hunan 411105, PR China

ARTICLE INFO

Article history:
Received 14 July 2009
Received in revised form 3 September 2009
Accepted 9 September 2009
Available online 16 September 2009

Keywords:
Supercapacitor
Polyaniline
Doped activated carbon
X-ray photoelectron spectroscopy
Electrochemical properties

ABSTRACT

A novel doped activated carbon has been prepared from H_2SO_4-doped polyaniline which is prepared by the oxypolymerization of aniline. The morphology, surface chemical composition and surface area of the carbon have been investigated by scanning electron microscope, X-ray photoelectron spectroscopy and Brunaner–Emmett–Teller measurement, respectively. Electrochemical properties of the doped activated carbon have been studied by cyclic voltammograms, galvanostatic charge/discharge, and electrochemical impedance spectroscopy measurements in 6 mol l^{-1} KOH. The specific capacitance of the carbon is as high as 235 F g^{-1}, the specific capacitance hardly decreases at a high current density 11 A g^{-1} after 10,000 cycles, which indicates that the carbon possesses excellent cycle durability and may be a promising candidate for supercapacitors.

1. Introduction

In recent years, supercapacitors (also called electrochemical capacitors) have attracted great attention as alternative energy-storage systems, compared to the conventional capacitors, they have higher energy density and broader range of working temperature; compared to the secondary battery, they have higher power density, longer cycle life (above 100,000 cycles), and shorter charging time [1–3]. Two kinds of supercapacitors have been studied: one is the electrical double-layer capacitor (EDLC), in which the capacitance arises from the charge separation at the electrode/electrolyte interface, such as carbon; the other is the pseudocapacitor, in which the capacitance arises from faradic reactions occurring at the electrode interface, such as transition-metal oxides [4–7] or electroactive polymers [8–11], etc. In the EDLC, the capacitance is proportional to the surface area of the electrode/electrolyte interface, in order to increase the specific capacitance, it is necessary to increase the surface area through increasing the micropores of the material, but it leads to the problem of ionic transportation. In pseudocapacitors, noble metal oxides [12–14] show high specific capacitance, but their application is limited by their high cost; Electroactive polymers also show high specific capacitance, but their application is limited by their poor chemical reversibility and short of cycling stability in aqueous electrolytes [15,16]. Literally, synergetic effects can be expected if the capacitive charging of the double-layer can be combined with a faradaic redox (pseudocapacitive) reaction in a way that both charge storage mechanisms work in parallel, with the overall capacitance of the electrode being the sum of the double-layer capacitance and the faradaic capacitance.

Introducing some functional groups containing many heteroatoms (such as oxygen, nitrogen, sulfur and halogen) into a carbon matrix is a good choice. The presence of these functionalities gives carbon materials an acid/base character [17,18], which enhances their capacitances by the pseudocapacitive effect. Recently, nitrogen-containing carbon materials have been reported as an interesting route to enhance capacitances [19–24]. The results showed that the extent of enhancement depended on the preparation route and electrolyte used.

In this paper, we have prepared a doped activated carbon derived from H_2SO_4-doped polyaniline which is prepared using the oxypolymerization method. Because polyaniline contains about 15 wt.% of nitrogen and 79 wt.% of carbon, it is commercially available and very cheap, we believe that it is a promising nitrogen-containing carbon material for supercapacitors. To the best of our knowledge, synthesizing such a carbon material for supercapacitors by this way has not yet been reported.

2. Experimental

2.1. Preparation of polyaniline

Aniline monomer was distilled prior to use, while other chemicals used were all analytical grade reagents. Distilled water was used in this experiment. A solution of 20 ml of aniline in 43 ml of

* Corresponding author. Fax: +86 731 58292251.
E-mail address: liuenhui99@sina.com.cn (E. Liu).

0378-7753/$ – see front matter © 2009 Elsevier B.V. All rights reserved.
doi:10.1016/j.jpowsour.2009.09.016

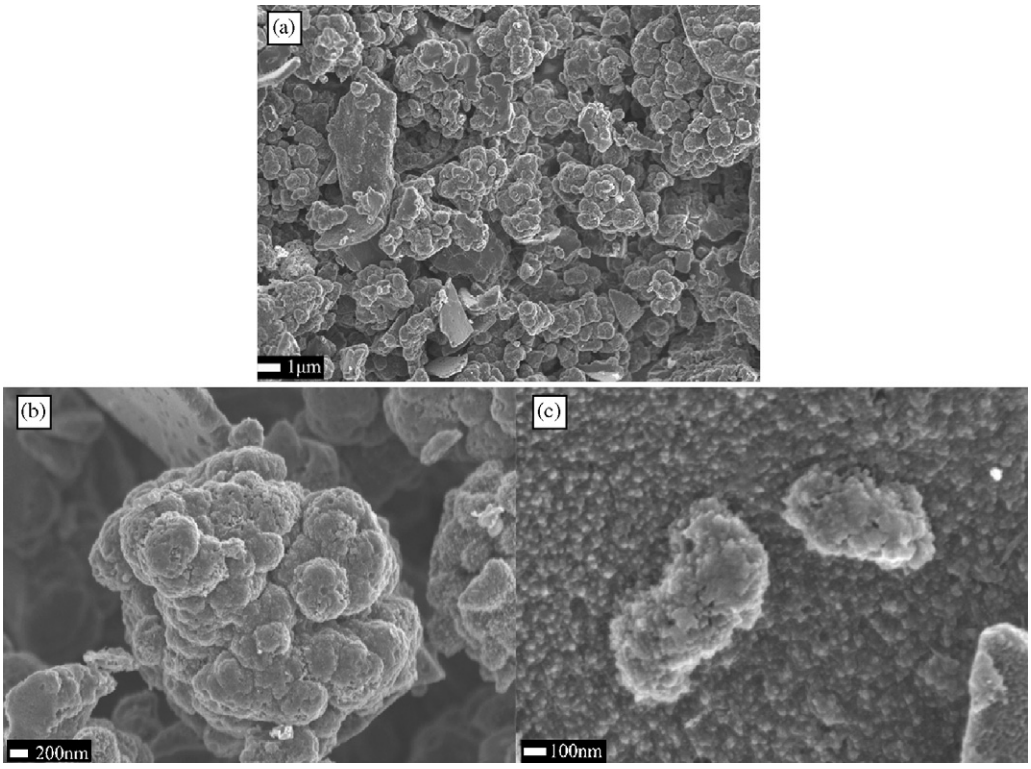

Fig. 1. SEM images of: (a) polyaniline, (b) carbon (C800) based on polyaniline and (c) activated carbon (CA800).

6 M H_2SO_4 was transferred to a three-neck flask, 20 ml $(NH_4)_2S_2O_8$ (APS) saturated solution was then added dropwisely into the above solution under vigorous stirring. After 30 min, 100 ml of APS saturated solution was then slowly added to the reaction mixture within 2 h. The polymerization reaction was continued for 4 h at room temperature. Finally the resulting green precipitates were filtered out, washed and dried at 100 °C for 48 h under vacuum condition.

2.2. Preparation of carbon materials

H_2SO_4-doped polyaniline was heated to 700, 800, and 900 °C at a heating rate of 5 °C min^{-1} under nitrogen flow and maintained at the desired temperature for 2 h. Afterward the carbon materials were activated by heating to 400 °C at a heating rate of 5 °C min^{-1} in mixed gas of oxygen and nitrogen (the volume percent of oxygen is 5%), the temperature at 400 °C was held for 2 h.

In order to facilitate the description in the text, carbon materials carbonized at 700, 800 and 900 °C under nitrogen are marked as series C (C700, C800 and C900), and then these carbon materials were activated at 400 °C with mixed gas of oxygen and nitrogen, we marked them as series CA (CA700, CA800 and CA900).

2.3. Materials characterization

Scanning electron microscope (SEM) measurements were performed on a Hitachi S5200 scanning electron microscope. The Brunaner–Emmett–Teller (BET) specific surface area and pore volumes of the carbon materials were determined by N_2 adsorption at 77 K on a Quantachrome NOVA-2200 system. The chemical state of the surface was characterized by X-ray photoelectron spectroscopy (XPS) on a VG Scientific ESCALAB 250 spectrometer with a Al Kα source. The spectra was charge corrected using the C1s peak (Eb (C1s) = 284.6 eV) as an internal standard. A non-linear, Shirley-type baseline and an iterative least-squares fitting algorithm were used to decompose the peaks, the curves being taken as 80% Gaussian and 20% Lorenzian. The surface atomic ratios were calculated from the ratio of the corresponding peak areas after correction with the theoretical sensitivity factors based on the Scofield's photoionization cross-sections.

2.4. Electrochemical testing

The electrochemical performances of all carbon samples were investigated using two-electrode Swagelok-type cells without a reference electrode. The electrode was fabricated by pressing a mixture of 80 wt.% carbon sample, 10 wt.% acetylene black, and 10 wt.% polyvinylidene fluoride (PVDF) onto a piece of nickel foil. Two electrodes with identical or very close masses were selected and then assembled as supercapacitors. The electrolytic solution was 6 M KOH. Cyclic voltammograms (CV) were recorded from 0 to 1 V at various sweep rates, discharge–charge curves were recorded from 0 to 1 V loading different current densities and electrochemical impedance spectroscopy (EIS) measurements were carried out by applying an AC voltage of 5 mV amplitude in the 100 kHz to 10 mHz frequency range using a CHI 660A electrochemical workstation (CHI Inc., USA). All electrochemical measurements were carried out at room temperature.

The specific capacitance of the electrode is obtained from Eq. (1):

$$C_g = \frac{I\Delta t}{m\Delta V} \times 2 \quad (1)$$

where C_g is the specific gravimetric capacitance (F g^{-1}), I is the current loaded, Δt is the discharge time (s), ΔV is the potential change during the discharge process (1 V in this study), and m (g) represents the mass of electroactive material.

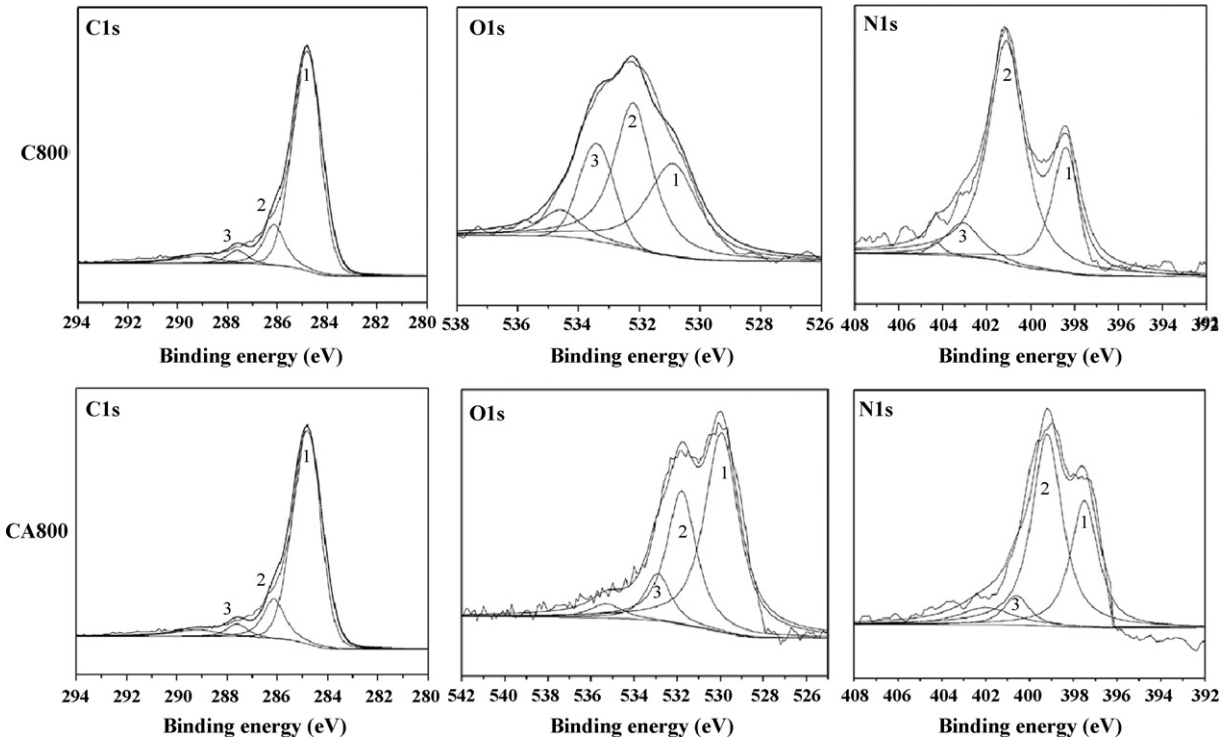

Fig. 2. X-ray photoelectron spectra of C800 and CA800.

Specific capacitances per surface area C_{SA} ($F\,m^{-2}$) were also calculated using Eq. (2):

$$C_{SA} = \frac{C_g}{SA} \quad (2)$$

where SA is a total surface area ($m^2\,g^{-1}$).

3. Results and discussion

3.1. SEM

Fig. 1(a) depicts representative SEM of polyaniline, it is schistose, and a lot of schistose polyaniline stack together. The morphology of carbon materials based on polyaniline (C800) is similar to which of polyaniline (Fig. 1(b)). The morphology of the activated carbon materials at 400 °C in mixed gas of oxygen and nitrogen (CA800) is granular, it is different from which of C800 (Fig. 1(c)), nanoparticles evenly distributed and the average diameter is about 30 nm. The reasons may be the breakage of some chemical bonds and partial oxidation of carbon surface.

3.2. XPS

The XPS spectrum of the as-prepared carbon indicates the presence of three distinct peaks, which can be explained by existence of carbon, nitrogen, and oxygen atoms. Fitting of the C1s spectrum (Fig. 2) can be resolved into three individual component peaks at binding energy of 284.7, 287.1 and 289.5 eV, representing graphitic carbon, carbonyl group and carboxyl group, respectively [25]. O1s spectrum is also shown in Fig. 2, the binding energies about 531, 532 and 533 eV represent C=O groups, C–OH groups and/or C–O–C groups, and chemisorbed oxygen (COOH carboxylic groups) and/or water, respectively. According to the literature [26–29], the chemical state of nitrogen atoms in graphene structure could be assigned to four types: N-6 (pyridinic nitrogen, 398.7 ± 0.3 eV), N-5 (pyrrolic nitrogen and pyridone nitrogen in association with oxygen functionality, 400.3 ± 0.3 eV), N-Q (quaternary nitrogen, nitrogen substituted with carbons in the aromatic grapheme structure, 401.4 ± 0.5 eV), N-X (pyridine-N-oxide, 402–405 eV). Except for the N-Q, all nitrogen functionalities are located at the edges of graphene layers. The peak analyses of N1s for the activated and unactivated samples revealed the presence of the same four contributions, but with different relative contributions. The ratios of pyridinic, pyrrolic, quaternary, and oxidized nitrogen for both samples are summarized in Table 1. The main conclusion of the peak deconvolution analysis is that CA800 contains slightly larger amounts of pyridinic and pyrrolic nitrogen as compared to C800. In addition, CA800 contains less content of C, more content of N and O.

3.3. Electrochemical properties of carbon electrodes

CV was used in determination of electrochemical properties of as-prepared samples. Fig. 3(a) shows the CV plots of all samples (activated and unactivated samples) at a sweep rate of $2\,mV\,s^{-1}$ with the potential range of 0–1 V. At this sweep rate all CV curves

Table 1
Surface composition and nitrogen form distribution in C800 and CA800.

Sample	Atomic concentration						Nitrogen form distribution			
	C	N	O	N/C	O/C	N/O	N-6	N-5	N-Q	N-X
C800	85.84	6.7	7.46	0.078	0.087	0.89	26.7	44.9	17.5	10.9
CA800	80.98	10.89	8.13	0.134	0.101	1.34	37.4	49.1	9.6	3.9

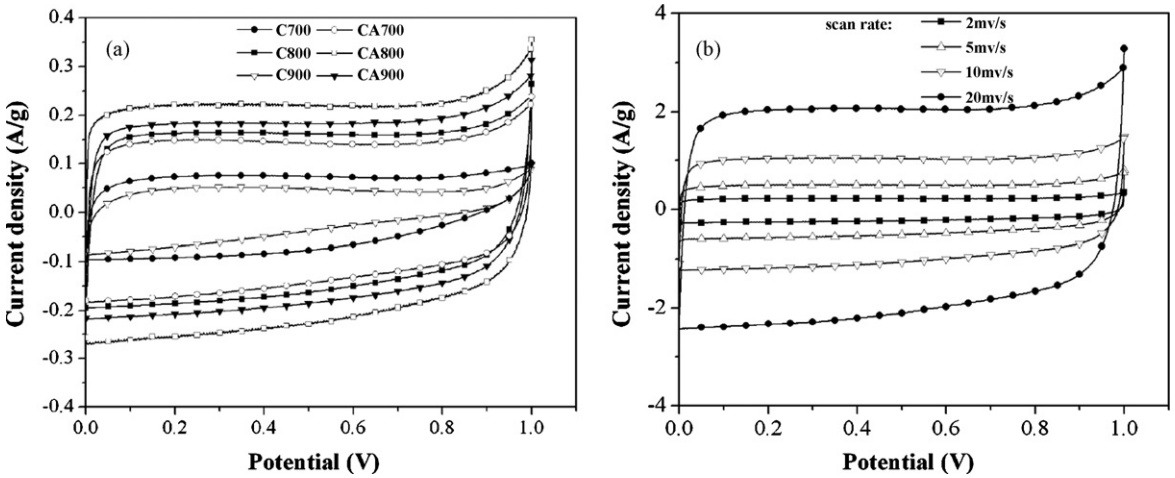

Fig. 3. Cyclic voltammograms of carbon electrodes in 6 M KOH electrolyte: (a) unactivated samples and activated samples at a scan rate of 2 mV s^{-1} and (b) CA800 samples with different scan rates.

exhibit near rectangular shapes with slightly distorted, which is characteristic of electrochemical capacitor. The range of current density of activated samples is higher than that of correspondingly unactivated samples, which indicates the activated samples have higher specific capacitance. The CV curve of CA800 exhibits bigger current response and larger area of rectangle than that of others, suggesting CA800 has higher specific capacitance. The CVs of the CA800 electrode material at different sweep rates are shown in Fig. 3(b). At 2, 5 and 10 mV s^{-1}, the curves present the typical rectangle "box-like" shape for charge/discharge process. At higher scan rates, for example, at 20 mV s^{-1}, the shape of the curve is still satisfactory, which indicates quick dynamics of charge propagation with this kind of carbon. It also suggests that CA800 can be excellent candidate as electrode materials for supercapacitor.

Galvanostatic charge/discharge measurements have also been conducted in order to investigate the electrode performance of CA800. The sample C800 was used as a contrast. The galvanostatic curves at a loading current density of 1 A g^{-1} are shown in Fig. 4. Both C800 and CA800 present a linear galvanostatic charge/discharge curve without obvious ohmic drop, indicating that both of them possess a good capacitive behavior under this loading current density. However, the specific capacitance of CA800 reaches 235 F g^{-1}, much larger than that of the C800 (141 F g^{-1}). The capacitance of CA800 can still remain 158 F g^{-1} even at a high loading current density of 11 A g^{-1} (Fig. 5), which can attribute to its quite small equivalent series resistance (ESR) for the ionic diffusion at a high speed.

High electrochemical stability of CA800 electrode is depicted in Fig. 5 by continuous galvanostatic charge/discharge cycling with different current densities in a symmetric capacitor which is charged up to 1 V. A little increase of specific capacitance occurs during the first 500 cycles, which was due to electrochemical activation, and thereafter the capacitance tends to be stable at 1, 3, 5, 7, 9, and 11 A g^{-1} current densities. At higher current densities, for example, 9 and 11 A g^{-1}, a little decrease of specific capacitance mainly occurs at the initial 2000 cycles, and thereafter the specific capacitance tends to stabilize. After 10,000 cycles, the specific capacitance is still about 99.9% of the initial specific capacitance, which indicates the sample possesses excellent cycle durability. It may be because the pseudocapacitance effect introduced by oxygen and nitrogen is stable with cycling. In addition, due to the low specific surface area of the material, the number of active sites that contribute to the electrolyte decomposition is very limited, the cycleability is improved [30].

EIS was utilized to obtain information on the supercapacitors' performance, such as their frequency dependence and ESR [25]. Fig. 6 illustrates the Nyquist plots of the C800 and CA800 supercapacitors. In all cases, a semicircle of very small radius is obtained at high-frequency region and a straight line in the low frequency

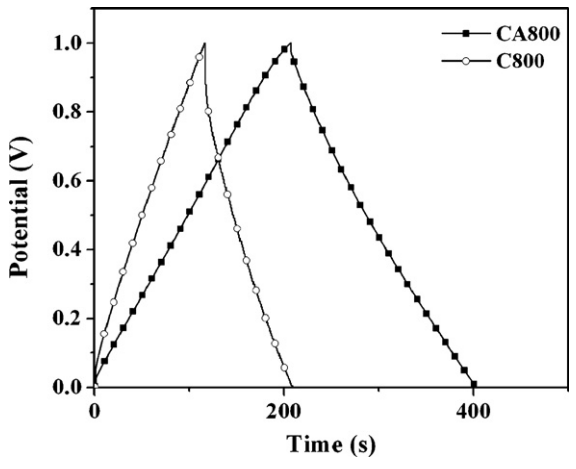

Fig. 4. Charge/discharge curves of C800 and CA800 samples at the current density of 1.0 A g^{-1}.

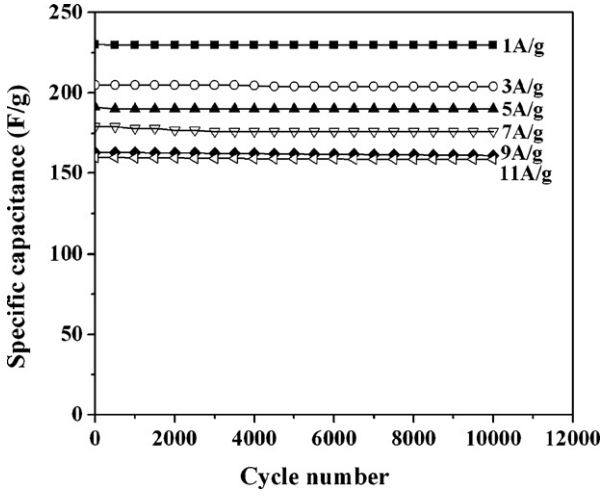

Fig. 5. Cycle behaviors of CA800 at the different current densities.

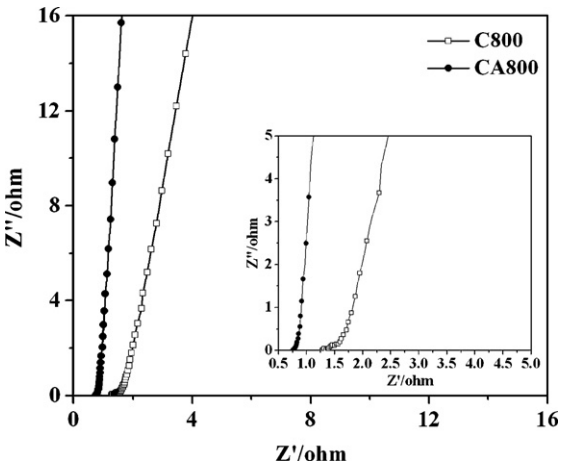

Fig. 6. Nyquist plot of C800 and CA800 (inset: enlarged high-frequency region of Nyquist plot).

region. At very high frequencies, the intercept at the real axis is the ESR value, the ESR value of C800 is obviously bigger than CA800's (CA800's is about 0.75, while C800's is 1.3 Ω), the reason may be that activated carbon materials generate a number of polar groups which results in the increase of the electric conductivity. The imaginary part of the impedance spectra at low frequencies represents the capacitive behavior of the electrode and approaches a 90° vertical line in an ideal capacitor [1]. Obviously, the straight line part of carbon CA800 is more close to vertical line along the imaginary axis, suggesting this carbon has better capacitive behavior than C800.

In order to investigate the reason of the increase of capacitance, BET test was used. The N_2 adsorption isotherms of C800 and CA800 are shown in Fig. 7. According to the IUPAC classification, the N_2 adsorption isotherms of both carbons exhibit type I characteristics, confirming their microporous character. CA800 has higher N_2 adsorption, which suggests an increase in pore volume and surface area for CA800 compared to C800. The surface area of CA800 is 514 $m^2\,g^{-1}$, which is bigger than C800's (325 $m^2\,g^{-1}$), suggesting surface area can be increased by activation in mixed gas of oxygen and nitrogen (see Table 2 and Fig. 1), the increase of surface area can improve the capacitance.

According to the literature [19,22,23], the presence of nitrogen atom group can offer carbon materials a base character, which is proportional to the nitrogen content. Heteroatoms polar functional group can improve the wettability of carbon material. Thus

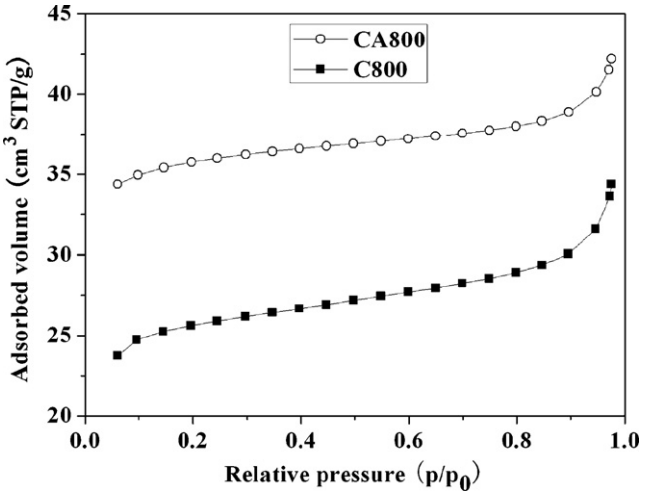

Fig. 7. N_2 adsorption isotherms of C800 and CA800.

Table 2
Surface characterization of C800 and CA800.

Sample	BET ($m^2\,g^{-1}$)	Pore volume ($cm^3\,g^{-1}$)	C_g ($F\,g^{-1}$)	C_{SA} ($F\,m^{-2}$)
C800	325	0.080	135	0.394
CA800	514	0.089	235	0.447

increasing the surface area is accessible to electrolyte or hydrated molecules for double-layer formation. The more heteroatoms polar functional group of N and O can offer more redox reactions in carbon matrix, suggesting more pseudocapacitance was produced. In this study, the CA800 shows less content of C, more content of N and O than C800 in Table 1. Therefore, we believe that increased specific capacitance may be attributed to synergic effects of pseudocapacitive and double-layer capacitance. Moreover, specific capacitance per surface area of CA800 and C800 was up to 0.447 and 0.394 $F\,m^{-2}$, respectively, which is bigger than commercial activated carbon (Maxsorb) [30] and activated carbon by other methods [27,30–33].

4. Conclusions

To summarize, we have prepared a doped activated carbon from H_2SO_4-doped polyaniline by carbonization and activation. To the best of our knowledge, it is the first time that a polyaniline-derived carbon has been prepared with the characteristics of low surface area and large heteroatoms (nitrogen and oxygen). Two kinds of capacitance contribution are involved in this material: one kind comes from the formation of the electrical double-layer, the other comes from pseudocapacitive effect caused by the presence of nitrogenated and oxygenated functionalities. The specific capacitance of the doped activated carbon material is as high as 235 $F\,g^{-1}$, the specific capacitance hardly decreases at a high current density 11 $A\,g^{-1}$ after 10,000 cycles. The advantages of this material are: (1) easy and fast synthesis; (2) easy handling compared with other powder carbon; (3) excellent performance (high specific capacitance and excellent cycling stability); (4) environmental benignity. All these characteristics testify that the doped activated carbon material may be a promising candidate for supercapacitors.

Acknowledgement

The authors are grateful for Project supported by Hunan Provincial Natural Science Foundation of China (07JJ6015).

References

[1] B.E. Conway, Electrochemical Supercapacitors: Scientific Fundamentals and Technological Applications, Kluwer Academic Plenum Publisher, New York, 1999.
[2] A. Du Pasquier, I. Plitz, J. Gural, F. Badway, G.G. Amatucci, J. Power Sources 136 (2004) 160–170.
[3] A.K. Cuentas-Gallegos, M. Lira-Cantú, N. Casañ-Pastor, P. Gómez-Romero, Adv. Funct. Mater. 15 (2005) 1125–1133.
[4] D. Choi, G.E. Blomgren, P.N. Kumta, Adv. Mater. 18 (2006) 1178–1182.
[5] C. Yu, L. Zhang, J. Shi, J. Zhao, J. Gao, D. Yan, Adv. Funct. Mater. 18 (2008) 1544–1554.
[6] R.P. Kalakodimi, K. Kazumichi, M. Norio, Chem. Mater. 16 (2004) 1845–1847.
[7] C. Xu, B. Li, H. Du, F. Kang, Y. Zeng, J. Power Sources 184 (2008) 691–694.
[8] S. Ghosh, O. Inganäs, Adv. Mater. 11 (1999) 1214–1218.
[9] L.Z. Fan, Y.S. Hu, J. Maier, P. Adelhelm, B. Smarsly, M. Antonietti, Adv. Funct. Mater. 17 (2007) 3083–3087.
[10] S. Palaniappan, S.L. Devi, J. Appl. Polym. Sci. 107 (2008) 1887–1892.
[11] W. Sugimoto, H. Iwata, Y. Yasunaga, Y. Murakami, Y. Takasu, Angew. Chem. Int. Ed. 42 (2003) 4092–4096.
[12] J.P. Zheng, Electrochem. Solid State 2 (1999) 359–361.
[13] C.C. Hu, W.C. Chen, K.H. Chang, J. Electrochem. Soc. 151 (2004) A281–A290.
[14] C.C. Hu, K.H. Chang, M.C. Lin, Y.T. Wu, Nano Lett. 6 (2006) 2690–2695.
[15] S.K. Mondal, K. Barai, N. Munichandraiah, Electrochim. Acta 52 (2007) 3258–3264.
[16] R. Pauliukaite, C.M. Brett, A.P. Monkman, Electrochim. Acta 50 (2004) 159–167.
[17] H. Tamon, M. Okazak, Carbon 34 (1996) 741–746.
[18] C.A. Toles, W.E. Marshall, M.M. Johns, Carbon 37 (1999) 1207–1214.

[19] Y.J. Kim, Y. Abe, T. Yanagiura, K.C. Park, M. Shimizu, T. Iwazaki, et al., Carbon 45 (2007) 2116–2125.
[20] K.W. Leitner, B. Gollas, M. Winter, J.O. Besenhard, Electrochim. Acta 50 (2004) 199–204.
[21] K. Jurewicz, K. Babel, A. Źiółkowski, H. Wachowska, Electrochim. Acta 48 (2003) 1491–1498.
[22] K. Jurewicz, R. Pietrzak, P. Nowicki, H. Wachowska, Electrochim. Acta 53 (2008) 5469–5475.
[23] H. Denisa, Y. Junya, S. Yasushi, H. Hiroaki, K. Masaya, Chem. Mater. 17 (2005) 1241–1247.
[24] K. Jurewicz, K. Babeł, A. Ziółkowski, H. Wachowska, J. Phys. Chem. Solids 65 (2004) 269–273.
[25] S. Biniak, G. Szymański, J. Siedlewski, A. Swiatkowski, Carbon 35 (1997) 1799–1810.
[26] F. Kapteijn, J.A. Moulijn, S. Matzner, H.P. Boehm, Carbon 37 (1999) 1143–1150.
[27] A. Bagreev, J.A. Menendez, I. Dukhno, Y. Tarasenko, T.J. Bandosz, Carbon 42 (2004) 469–476.
[28] K. Jurewicz, K. Babel, A. Ziolkowski, H. Wachowska, Electrochim. Acta 48 (2003) 1491–1498.
[29] K. Jurewicz, K. Babel, A. Ziolkowski, H. Wachowska, J. Phys. Chem. Solids 65 (2004) 269–273.
[30] E. Raymundo-Piñero, F. Leroux, F. Béguin, Adv. Mater. 18 (2006) 1877–1882.
[31] K. Jurewicza, R. Pietrzakb, P. Nowicki, H. Wachowska, Electrochim. Acta 53 (2006) 5469–5475.
[32] G. Lota, B. Grzyb, H. Machnikowska, J. Machnikowski, E. Frackowiak, Chem. Phys. Lett. 404 (2005) 53–58.
[33] V. Subramanian, C. Luo, A.M. Stephan, K.S. Nahm, S. Thomas, B. Wei, J. Phys. Chem. C 111 (2007) 7527–7531.